Composite Structures 337 (2024) 118076

Contents lists available at ScienceDirect

Composite Structures

journal homepage: www.elsevier.com/locate/compstruct

Multifunctional composite material based on piezoelectric nanofibers and Cu-CFRP electrodes for sensing applications

Francesco Mongioì [a], Giacomo Selleri [b,*], Tommaso Maria Brugo [a,*], Emanuele Maccaferri [c], Davide Fabiani [b], Andrea Zucchelli [c]

[a] Department of Industrial Engineering, University of Bologna, Viale Risorgimento 2, 40136 Bologna, Italy
[b] Department of Electrical, Electronic, and Information Engineering, University of Bologna, Viale Risorgimento 2, 40136 Bologna, Italy
[c] Department of Industrial Chemistry "Toso Montanari", University of Bologna, Viale Risorgimento 4, 40136 Bologna, Italy

ARTICLE INFO

Keywords:
Piezoelectricity
P(VDF-TrFE) nanofibers
Composites
Smart materials
Response surface method

ABSTRACT

To monitor possible failures of a composite, several Structural Health Monitoring (SHM) systems have been developed. However, these methods typically involve embedding commercial sensors within the laminate, potentially compromising the material's strength.

In this study, a self-sensing composite laminate was fabricated by interleaving poly(vinylidenefluoride-trifluoroethylene) (P(VDF-TrFE)) piezoelectric nanofibers between Glass Fiber Reinforced Plastic (GFRP) pre-preg plies. Instead of conventional metallic sheets, hybrid Copper-Carbon Fiber Reinforced Plastic (Cu-CFRP) was used as electrodes to collect piezoelectric signals. This innovative approach offers two main advantages: enhanced interlaminar fracture toughness due to nanometric piezoelectric fibers and an intrinsic connection between copper wires and carbon, eliminating the need for additional electrical cables within the laminate. The effect of stacking sequence parameters on the self-sensing laminate's electromechanical response was investigated using a Design of Experiment (DoE) based on the Box-Benken method. Additionally, a lumped electric circuit model was employed to gain analytical insights into the piezoelectric behavior of the laminates.

1. Introduction

Throughout the last few decades, the use of Fiber-Reinforced Plastics (FRP) has rapidly increased, thanks to their high specific stiffness and strength compared to traditional materials such as metals. However, components made of FRP laminates are prone to delamination when subjected to out-of-plane loads, due to their laminar morphology. Cracks caused by impact often develop within the laminate without any visible damage on the surface [1], until reaching a critical size that leads to the sudden and catastrophic failure of the component.

In order to avoid critical failures, there is a tendency to oversize the component and to periodically inspect it via non-destructive tests (NDT). Such tests require high maintenance costs and long machine downtime [2]. Therefore, several Structural Health Monitoring (SHM) systems have been developed to monitor in real-time the structural integrity of the component. These kinds of systems require the use of sensors, which can be embedded into the laminate or externally mounted on it. External sensors usually do not affect the mechanical performances of the laminate; however the exposure to external environmental conditions, electronic interferences and impacts could affect their proper functionality [2]. For these reasons, it is often preferable to interleave the sensors between the laminate plies. Sensors based on the Fiber Bragg Grating (FBG) [3–5] and piezoelectric ceramic-based wafers, such as lead zirconate titanate (PZT) [67], can be integrated within the laminate. The main drawbacks with inserting extrinsic sensors within the laminate concern their sub-millimetric size, (much larger than the size of the reinforcing fibers) and the elastic properties mismatches. When inserting FBG-based sensors, the formation of an eye-shaped pocket could trigger cracks which may develop through the layers perpendicularly to the reinforcement fibers [8]. In the case of PZT breakage, the presence of PZT wafers within the laminate leads to trigger points due to its extremely brittle ceramic nature [9]. The aforementioned methods to make self-sensing laminates have very high sensitivity in strain detection [10] and impact localization, using Lamb waves [11], but they create likely crack initiation zones in the component [8]. One possible solution is to reduce the size of the sensing active

* Corresponding authors.
E-mail addresses: giacomo.selleri2@unibo.it (G. Selleri), tommasomaria.brugo@unibo.it (T. Maria Brugo).

https://doi.org/10.1016/j.compstruct.2024.118076
Received 29 September 2023; Received in revised form 19 March 2024; Accepted 21 March 2024
Available online 26 March 2024

material to the nano-scale dimension and disperse it in the hosting material [12]. For instance, carbon nanotubes (CNTs) have been used to make the matrix electrically conductive and to confer it piezoresistive properties [13–15] and PZT nano-powders have been interleaved between the FRP plies to make the laminate piezoelectrically active, without affecting its inherent strength [16 17]. Another possible way is to use polymeric piezoelectric materials, such as polyvinylidene fluoride (PVDF) and its copolymers [18,19], which has excellent flexibility and internal dumping [20,21]. To avoid adhesion issues, it can be useful to embed the active material in the form of nanofibrous mat [22,23]. The electrospinning process allows to obtain nanofiber mats of many types of polymers [24], among which PVDF [25–27]. Some works demonstrated an increase of the composite toughness by adding a negligible amount of electrospun material, due to the random texture of the nanofibers and the high ductility of some polymers [28–31]. However, embedding piezoelectric materials into a composite laminate poses issues regarding the alignment of the ferroelectric dipoles in a main direction and a poling process is required to confer a macroscale piezoelectric behavior to the composite material [25,26]. Usually, the poling process is performed by applying an external electric field to the whole laminate (in-situ polarization). However, the presence of embedding dielectric material could impact on the polarization effectiveness [32–34]. Therefore, to maximize the piezoelectric coefficient of the nanofiber mat and to avoid electrical discharges during the in-situ polarization, alternative poling techniques have been developed, such as corona poling [35–38]. To complete the structure of the self-sensing laminate, electrodes are needed to collect the piezoelectric signal [12,16,22]. Traditionally, several works in literature reported about the intercalation of metallic layers (i.e., aluminum sheets or copper foils) between the laminate plies, but adhesion issues could occur at the interface with the resin due to the elastic properties mismatch. Subsequently, recent works exploited the electrical conductivity of the carbon fibers [39] to extract the piezoelectric signal, by using a copper tape which connects the carbon fibers to the signal cables [40]. In this way, carbon fibers are exploited by combining their mechanical and electrical properties.

In this study, the composite laminate was made piezoelectrically active by interleaving a poly(vinylidenefluoride-trifluoroethylene) P(VDF-TrFE) nanofibrous mat between the Glass Fiber Reinforced Plastic (GFRP) plies. Prior to embedding, the nanofibers were polarized through the corona poling process. A primary pair of Carbon Fiber Reinforced Plastic woven with copper wires (Cu-CFRP) layers served as signal electrodes for the acquisition of the piezoelectric signal. Additionally, an auxiliary pair of Cu-CFRP plies was externally introduced to provide shielding against triboelectric noise and electromagnetic interference (EMI) [41]. The use of such electrodes instead of metallic sheets allows to reduce adhesion issues, thus combining their mechanical and electrical properties. Through a Design of Experiment (DoE), the effect of P(VDF-TrFE) grammage and the number of GFRP plies in the composite laminate on the electromechanical response was analyzed. The DoE led to the definition of a response surface which fully described the effect of each parameter on the piezoelectric performances. A lumped electric model was developed to provide valuable insights into the sensor behavior by using the electrical, mechanical and geometrical properties of the single constituents.

2. Materials and methods

2.1. Fabrication process of the self-sensing laminate

2.1.1. Electrodes manufacturing

Despite the high conductivity of conventional metal electrodes, their incorporation into composite laminates can result in mechanical delamination, primarily due to the disparity in elastic properties and adhesion issues with the epoxy matrix. A novel aspect in this work lies in the utilization of electrodes harnessing the electrical conductivity of carbon fibers.

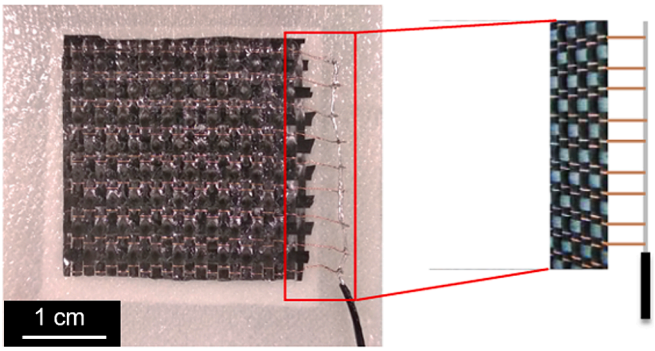

Fig. 1. Cu-CFRP electrode with copper wires.

The Cu-CFRP electrodes are made of prepreg with carbon fiber plain woven fabric, directly braided by the supplier with 0.1 mm diameter copper wires with 3.5 mm step during the weaving process and epoxy matrix (PW T300 200 g/m^2 - epoxy matrix, hybrid fabrics GGCu270-P by G. Angeloni S.r.l.), as shown in Fig. 1. Thanks to the relatively high conductivity of the carbon fibers (0.6*10^3 S/cm) and the dense structure of the fiber fabric, the piezoelectric signal generated by P(VDF-TrFE) is initially captured by the carbon fibers and subsequently transferred to the copper wires (0.6*10^6 S/cm). Afterwards, the segments of copper wires at the periphery of the electrodes were connected to a signal cable coated with a Teflon jacket (430-FST, Micro-Measurements). This arrangement facilitates the transmission of the piezoelectric signal to the data acquisition system, as illustrated in Fig. 1.

It is noteworthy that the added weight of the copper wires is negligible in comparison to a conventional CFRP pre-preg. This configuration presents a promising strategy for substituting traditional metallic electrodes with a material that does not compromise the mechanical performance of the laminate.

2.1.2. Electrospinning process

The piezoelectric nanofibrous non-woven mat was fabricated by electrospinning method, starting from a polymeric solution prepared by dissolving 7 wt% of the copolymer P(VDF-TrFE) (80/20 mol%, Mw = 600 kDa, kindly provided by Solvay S.p.A. Milan, Italy, https://www.solvay.com) in dimethylformamide (DMF) (23 wt%) and acetone (70 wt%). The copolymer shows a Curie temperature (T_c) of 133 °C and a melting temperature (T_m) of 145 °C. The non-woven nanofibrous mat was fabricated with a four needle - drum collector electrospinning machine (Lab Unit, Spinbow®, [31]) by applying 16 kV to the high-voltage needles and collecting the randomly oriented nanofibers on the grounded rotating drum (0.2 m/s tangential speed), which was placed 16 cm away from the needles. The electrospinning process was carried out with a flow rate equal to 0.8 ml/h per nozzle, at 24 °C and 40 % of relativity humidity (RH).

Since this work aims to investigate and model the effect of different volumetric fractions of the piezoelectric phase on the electrical response of the self-sensing composite laminate, three nanofibrous membranes with different grammages were fabricated. In particular, the electrospinning process took place for 5, 10 and 18 h to produce A3 size randomly oriented nanofibrous mats with a nominal grammage of 10, 20 and 30 g/m^2, respectively.

2.1.3. Poling

The piezoelectric nanofibers were polarized before the integration with the composite material by corona poling [38]. In this method, the electric charges are generated from a needle connected to a high-voltage generator and flow towards a ground electrode [42]. By disposing the piezo-polymer on the ground plate, the ions are sprayed from the needles and deposit on the nanofibers, thus inducing the alignment of the dipoles. This technique, compared to the in-situ polarization of the

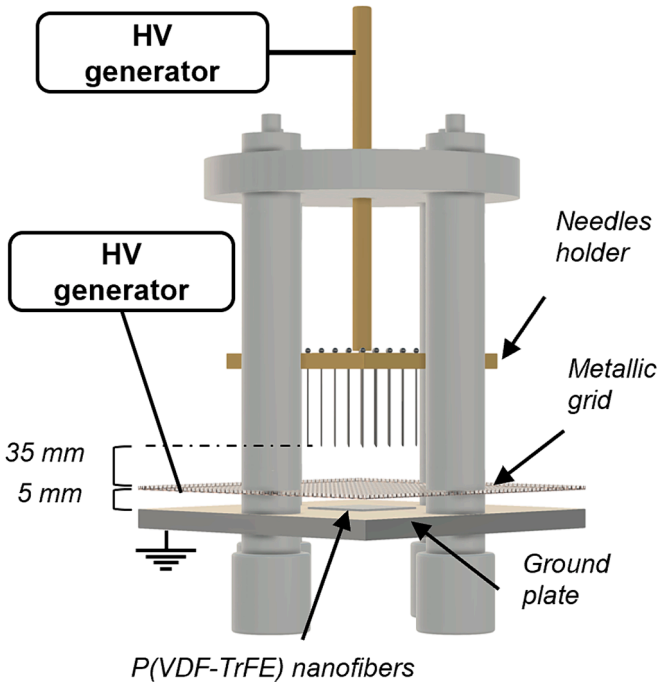

Fig. 2. Corona cell polarization setup.

nanofibers embedded in the composite as performed in [22], allows to apply higher electric fields directly on the piezoelectric nanofibers [16,34].

As schematically represented in Fig. 2, the corona poling cell has been equipped with 25 needles equally spaced 1 cm apart on a brass needle holder. A metallic grid was inserted between the needles and the ground plate to optimize the ions distribution on the sample surface.

The parameters for a successful polarization of P(VDF-TrFE) nanofibers have been investigate in previous work [37]. Herein, since in this work the aim is to keep constant the d_{33} of all the nanofibrous membranes in order to reduce the experimental variables, the polarization parameters have been properly tuned for each different grammage. With this purpose, it can be observed that the high-voltage value applied to the needles increases with the grammage of the sample, due to the higher amount of insulating material between the needles and the ground. The temperature was set at 130 °C to favor the dipoles mobility. The process parameters were the following: HV grid = -3 kV, needles-grid distance = 35 mm, grid-ground distance = 5 mm, polarization time = 60 min and temperature = 130 °C. The HV value applied to the needles was set at −22, −24 and −26 kV for 10, 20 and 30 g/m^2, respectively.

Thickness measurements were performed on each nanofibrous mat grammage to verify any variation induced by the corona poling treatment. Five measurements were performed on each samples. Before corona poling, the thickness values were equal to 28.1 ± 3.2, 53.3 ± 5.4 and 71.4 ± 6.1 μm, for 10, 20 and 30 g/m^2, respectively. After the treatment, the values were equal to 25.2 ± 2.2, 48.3 ± 3.7, 68.6 ± 4.3 μm. Overall, after the corona poling a slight decrease of the thickness is observable, likely due to the electrostatic phenomena involved in the process. However, the maximum reduction is equal to 11.5 % in the case of Gr = 10 g/m^2, which can be considered negligible.

2.1.4. Design space and stacking sequence

To achieve a comprehensive understanding of the electromechanical behavior of a self-sensing composite laminate functionalized with piezoelectric nanofibers, an experimental campaign was designed to investigate the effects of different stacking sequences on laminate performance. For this purpose, a Design of Experiments (DoE) with three variation levels for each factor was deemed suitable (3^k factorial design) to explore up to a second-order effect.

According to [22] and [41], in real SHM applications to have a pure piezoelectric signal proportional to the impact force and avoid triboelectric noise and electromagnetic interferences shield electrodes are mandatory.

In this study, three primary factors were varied during the stacking sequence of the self-sensing laminate, as illustrated in the schematic representation in Fig. 3. These factors included the grammage of the piezoelectric nanofibrous layer (*Gr*), the number of GFRP plies between the signal electrodes (n_{int}) and the number of GFRP plies between the signal electrodes and the shield ones (n_{sh}). The grammage levels of the nanofibrous membranes (*Gr*) were 10, 20, and 30 g/m^2, as previously mentioned in Section 2.1.2, while the number of GFRP plies - both between the signal electrodes (n_{int}) and between the shield electrodes and the signal ones (n_{sh}) - was varied between 2, 4, and 6.

Executing a full 3^3 factorial design would necessitate at least 27 different specimen configurations, without considering any replications. To limit the number of samples to be fabricated and preserve the robustness of the experimental results, a Box-Behnken design (BBD) was employed [43]. This type of DoE allows a response surface to be modeled as a mathematical function of a few continuous factors, thereby reducing the number of sample configurations from 27 to 12 [44]. Each factor's level was normalized as a coded value for clarity, as shown in Table 1. This codification process has been performed with the aim to generate a visual overview of the design space represented in Fig. 4 and to make clearer the impact of each factor on the response surface function described in detail in Section 3.3.

The variance of the whole manufacturing process was estimated by replicating three times the central point of the design space, which correspond to the sample with *Gr* = 20 g/m^2, n_{sh}=4 and n_{int} = 4. All the self-sensing laminates configurations fabricated in this work are summarized in Table 2.

As depicted in Fig. 3, each self-sensing laminate is symmetrical and comprises a piezoelectric nanofiber mat interleaved at the midplane (35 × 35 mm). The Cu-CFRP plies used as signal electrodes have dimensions of 30 × 30 mm and are interspersed with layers of woven GFRP prepreg (E-glass 8H Satin 300 g/m^2 - epoxy matrix, VV300S - DT121H-34 DeltaPreg, 50 × 50 × ~ 0.22 mm). Cu-CFRP shield electrodes were added to cover a larger area (40 × 40 mm) and were insulated from the signal electrodes by a variable number of GFRP plies (n_{sh}) [14].

After stacking all specimens of the BBD, they were cured in an autoclave with vacuum bag pressure of −850 mbar and external pressure of 6 bars, using a single-step cure cycle consisting of a 12-hour isotherm @ 80 °C and 1 °C/min heating and cooling ramps. The choice of a low curing isotherm value and slow heating ramp promoted the impregnation of the nanofiber mat by the GFRP epoxy matrix and

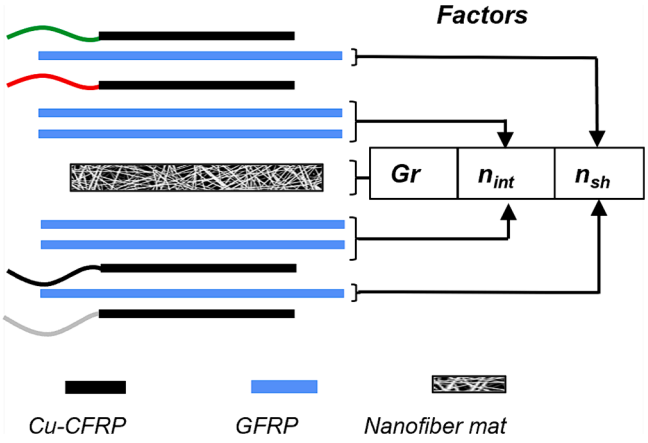

Fig. 3. Schematic representation of the self-sensing laminate and DoE factors.

Table 1
BBD variables and their values.

Variables		Level 1		Level 2		Level 3	
		Natural value	Coded value	Natural value	Coded value	Natural value	Coded value
P(VDF-TrFE) Grammage (g/m^2)	Gr	10	−1	20	0	30	1
GFRP between inner electrodes	n_{int}	2	−1	4	0	6	1
GFRP between signal and shielding electrodes	n_{sh}	2	−1	4	0	6	1

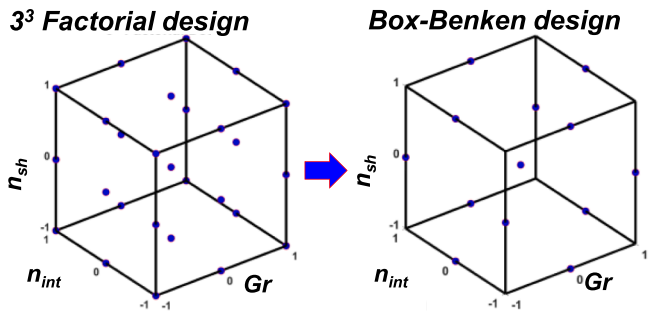

Fig. 4. Space variables of the 33 factorial design and the BBD.

ensured that the piezo-active material temperature remained below the P(VDF-TrFE) Curie one (T_c), preventing depolarization. The 6-bar pressure helped improve nanofiber interleaving and prevented the development of air inclusions into the laminates [22].

2.1.5. Signal conditioning

As a compressive load is applied on the self-sensing laminate, the electrical charges generated by the nanofibrous piezoelectric mat were collected by the two signal electrodes of the laminate. While the outer electrodes couple was connected to the ground to shield the sensors from triboelectric noise and electromagnetic interference (green and grey cables of Fig. 5). The electrical charges generated by the P(VDF-TrFE) membrane were collected by the two Cu-CFRP signal electrodes, transferred to the woven copper wires and then to the signal cables (red and black cables of Fig. 5). As well-known from the piezoelectric theory [32], the RC constant of the acquisition circuit determines the cut-off frequency of the sensor. In this work the piezoelectric signals were acquired above the cut-off frequency of the self-sensing laminates. Therefore, the piezoelectric signal was acquired by connecting the signal cables to an electrometer (Keithley 6517B) due to its high internal resistance (>200 TΩ), as shown in Fig. 5. The electromechanical characterization of the laminates was performed also without connecting the shield electrodes to the ground. In this case, the green and the grey cables were left floating.

2.2. Electrical characterization

2.2.1. Single constituents electrical characterization

The dielectric constants of the GFRP and P(VDF-TrFE) were measured a dielectric analyzer (Novocontrol alpha dielectric analyzer B2.2) in the frequency range of 10^{-2}–10^4 Hz.

To estimate the Cu-CRFP electrode resistance, a Cu-CFRP ply was interleaved between two plies of GFRP to reproduce the electrode configuration in the self-sensing composite. Along the two opposing edges of the laminate, seven signal cables were soldered to the woven copper wires. This was done to gauge the electrical resistance between the copper wires at various intervals, by using a RLC meter (Voltcraft LCR-100) as shown in Fig. 6a. The maximum recorded resistance value among the various pairs of cables amounted to 0.3 Ω. Therefore, it can be assumed that the Cu-CFRP ply works as an ideal conductor.

The piezoelectric strain coefficient (d_{33}) of the poled nanofibrous mat was evaluated by using a piezometer (Piezotest PM300, Fig. 6b).

2.2.2. Composite piezoelectric characterization

The capacitances of the self-sensing composite laminates were measured across the signal cables using an RLC meter (Voltcraft LCR-100). For each specimen, the capacitance was measured both by connecting the shield cables to the ground and by leaving them floating.

Afterwards, the piezoelectric output signals of the sensing laminates were evaluated with a compressive cyclic load using an Instron 8033 hydraulic testing machine equipped with a 25 kN load cell. As it is shown in Fig. 7, the specimens were compressed between a flat plastic support and plastic cylindrical indenter with a diameter of 10 mm. A sinusoidal compressive force oscillating between 0.6 and 1.1 kN at 20 Hz was applied on each specimen [32]. The applied compressive force and the piezoelectric signals were simultaneously acquired at a frequency of 2 kHz.

3. Results and discussion

3.1. Micrograph analyses

When interleaving a thin bulky film of P(VDF-TrFE) between the plies of a composite material, the presence of a weak interface between the epoxy matrix and the fluorinated polymer can trigger delamination in case of out-of-plane impacts. If the film is replaced by the nanofibers, during the curing cycle described in Section 2.1.4, the epoxy resin of the GFRP plies penetrates between the air pores of the nanofibrous membrane and fully impregnates it. In this way, an intimate contact between

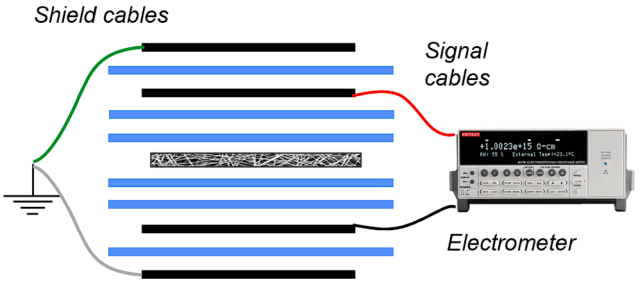

Fig. 5. Stacking sequence of the self-sensing laminate and electric connections.

Table 2
List of the configurations of the sensing laminate fabricated in this work.

ID	1	2	3	4	5	6	7	8	9	10	11	12	13	14	15
Gr	10	10	30	30	10	10	30	30	20	20	20	20	20	20	20
n_{int}	2	6	2	6	4	4	4	4	2	2	6	6	4	4	4
n_{sh}	4	4	4	4	2	6	2	6	2	6	2	6	4	4	4

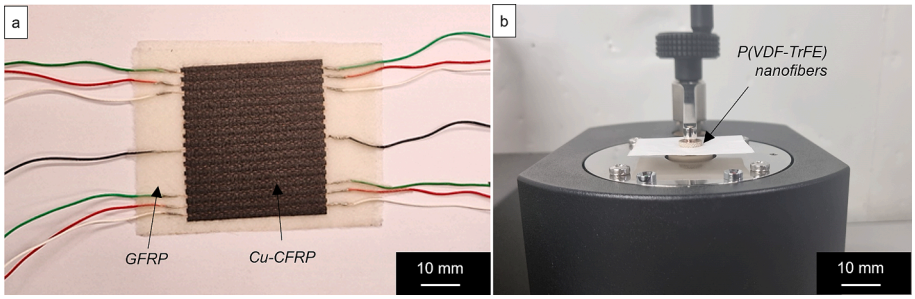

Fig. 6. a) Cu-CFRP resistance measurement and b) piezoelectric coefficient measurement setup.

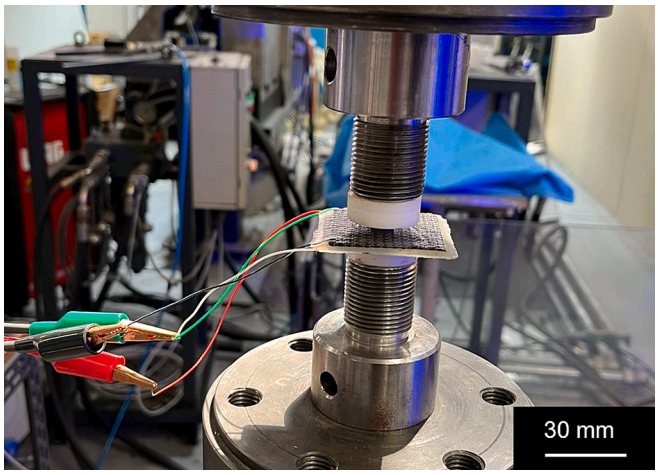

Fig. 7. Piezoelectric characterization setup.

the nanofibers and the surrounding hosting material is established, thus reducing the risk of delamination.

The morphology of the nanofiber membrane was analyzed via SEM image, as shown in Fig. 8. The electrospun PVDF-TrFE nanofibers are randomly oriented and bead-free. The average diameter of the nanofibers is equal to 516 ± 77 nm (calculated with the software ImageJ).

The integration mechanism of the nanofibers within the composite laminate has been investigated in this work by optical and SEM micrograph analyses of the cross section. The overall view of the central configuration laminate (ID_15) is shown in Fig. 9a. In particular, the stacking sequence is clearly visible with the thin layer of nanofibers located in the midplane. The Cu-CFRP electrodes can be distinguished from the GFRP plies through the presence of the copper wires, which are visible as white circles in Fig. 9a. In the SEM magnification of Fig. 9b and Fig. 9c the optimal impregnation of the nanofibers within the epoxy resin can be observed, without any voids or delamination between the piezoelectric material and the GFRP, creating an intimate contact with the adjacent GFRP plies. In addition, the specimen was then soaked for 30 min in an acetone bath to dissolve and remove the P(VDF-TrFE) nanofibers. In this way, the nanofibers appear as holes in the SEM magnification of Fig. 9d.

3.2. Electrical properties

3.2.1. Constituents electrical properties

The absolute permittivity (ε) of the single phases and the piezoelectric strain coefficient d_{33} of P(VDF-TrFE) 80/20, were measured according to the procedures described in Section 2.2.1 and their values are reported in Table 3. In particular, the permittivity values (ε^P and ε^G for P(VDF-TrFE) and GFRP, respectively) were determined for the regime state in the frequency domain, reached at 10^4 Hz. The

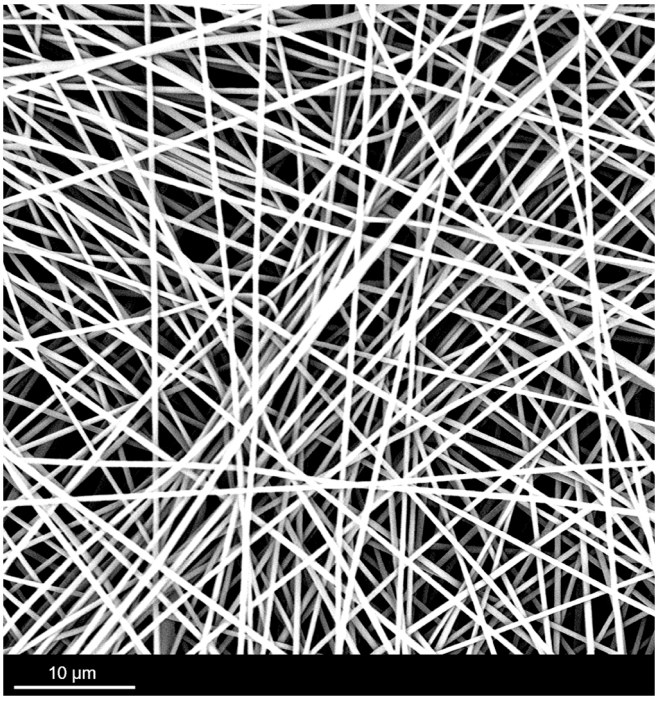

Fig. 8. SEM image of the electrospun nanofibrous membrane.

piezoelectric strain coefficient d_{33} was measured for each specimen and the mean value with the standard deviation is reported in Table 3.

3.2.2. Composite electrical properties

The capacitance values of the self-sensing composite laminates were measured according to the procedure described in Section 2.2.2 and are reported in experimental section of Table 4, both for the shielded (C^C_{shield}) and no-shielded ($C^C_{noshield}$) configurations. Generally, it is noticeable that the capacity values of the laminates with the grounded shield electrodes is systematically lower than the values of the no-shielded configuration. Moreover, by taking into account the no-shielded configuration, the more the number of GFRP plies between the signal electrodes, the lower the capacitance.

The sensitivity has been used as parameter to define the performances of the laminate as a sensor, and it was calculated as the ratio between the peak-to-peak output voltage and the peak-to-peak input compressive load. According to the procedure described in Section 2.2.2, the output voltage signal and the applied load are graphed in Fig. 10a and Fig. 10b for the ID_3 laminate ($Gr = 30$ g/m^2, n_{int}=2 and$n_{sh} = 6$), both for the shielded and no-shielded configuration, respectively. In shield connection case, the sensitivity was calculated as 44.9 mV/kN (S^C_{shield}), while the sensitivity of the no-shielded configuration ($S^C_{noshield}$) is equal to 54.4 mV/kN. This difference is discussed more in detail in Section 3.2.3.

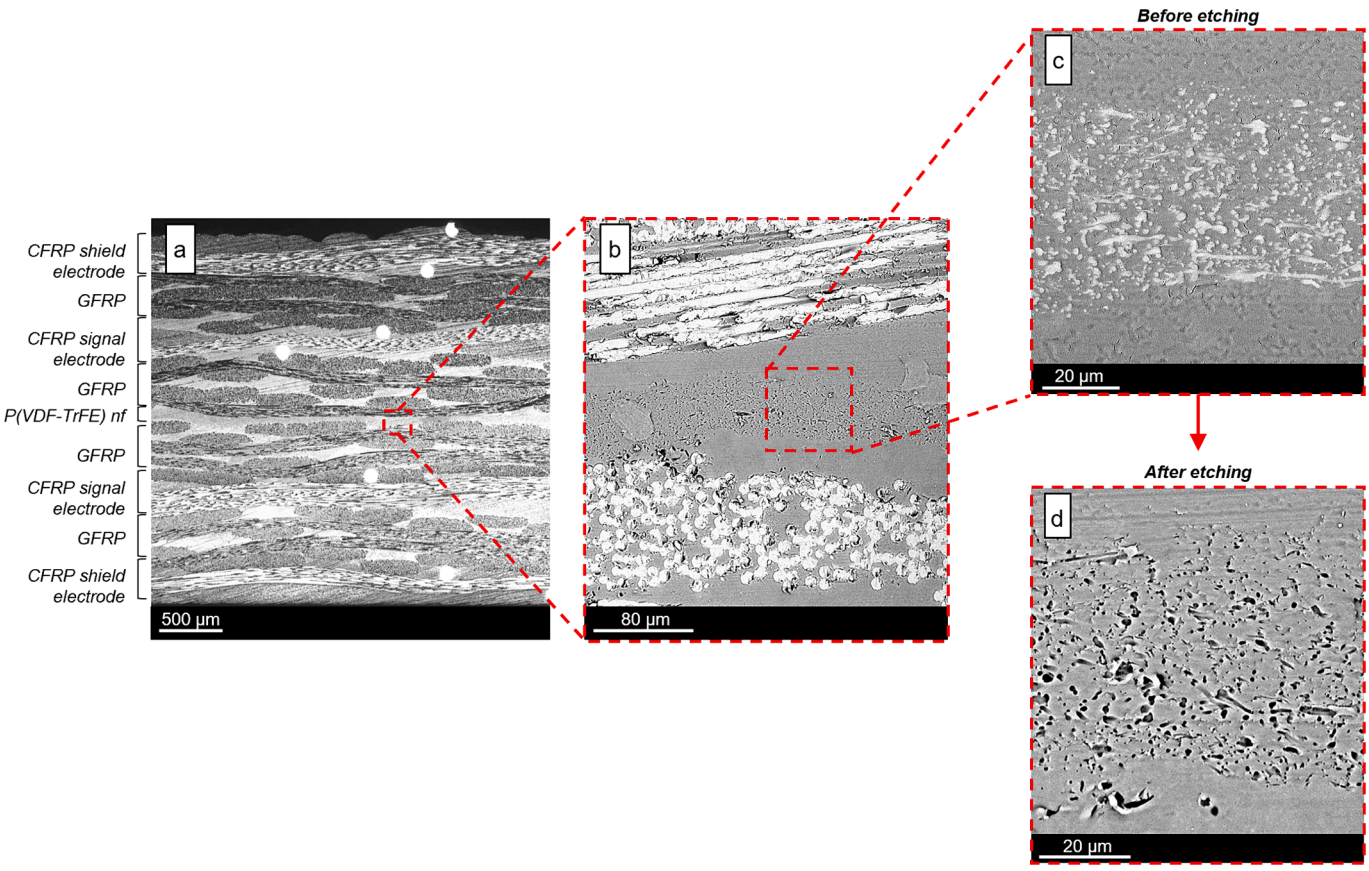

Fig. 9. a) Optical micrograph analysis of the cross-section of the self-sensing composite laminate and b) SEM magnifications c) before etching and d) after etching.

Table 3
Single-constituents electrical properties.

	ε (F/m 10^{-12})	d_{33}(pC/N)
P(VDF-TrFE)	67.7	8.2 ± 2.72
GFRP	58	/

The sensitivity values (S^C_{shield} and $S^C_{noshield}$) of all specimens fabricated in this work are summarized in the bar graph of Fig. 11. The error bars of the graph are the standard deviation value, calculated for the three times-replicated central configuration of the design space (laminate ID {13; 14; 15}). In the case of the shielded configuration, the standard deviation value is equal to 2.15 mV/kN, whereas it increases up to 7.67 mV/kN for the no-shielded configuration. This remarkable increment of the standard deviation value can be attributable to the presence of triboelectric effects or electromagnetic interference, which are not erased when the shield electrodes are not connected to the ground [41].

Table 4
Experimental vs model electrical parameters for each laminate. The first section groups all the parameters measured and calculated directly on the laminates of the two different testing conficurazions; The second section groups the predicted parameters by the lumped electrical circuit model. The apex (*) has been superimposed onto the parameters referring to the electrical circuit model.

Lam_ID	Experimental section						Lumped electrical circuit model			
	$C^C_{no\ shield}$(pF)	C^C_{shield}(pF)	$S^C_{no\ shield}$(mV/kN)	S^C_{shield}(mV/kN)	$d^C_{33_{no\ shield}}$(pC/N) $\times10^{-3}$	$d^C_{33_{shield}}$(pC/N) $\times10^{-3}$	$C^{C*}_{no\ shield}$(pF)	C^{C*}_{shield}(pF)	$S^{C*}_{no\ shield}$(mV/kN)	S^{C*}_{shield}(mV/kN)
1	94.7	116.0	21.4	20.5	2.02	2.38	104.6	130.8	19.4	18.2
2	48.6	77.5	14.8	11.0	0.721	0.853	34.9	61.0	20.7	14.0
3	98.0	122.0	54.4	44.9	5.33	5.48	104.6	130.8	51.0	41.9
4	45.6	73.2	28.9	22.2	1.32	1.63	34.9	61.0	37.8	26.6
5	74.2	132.0	16.3	11.6	1.21	1.53	52.3	104.6	23.1	14.6
6	61.2	80.2	22.9	16.1	1.40	1.29	52.3	69.8	26.8	18.5
7	72.3	100.0	25.8	20.8	1.87	2.08	52.3	104.6	35.7	19.9
8	56.7	73.4	38.4	31.7	2.18	2.33	52.3	69.8	41.6	33.4
9	103.0	149.0	39.4	30.0	4.06	4.47	104.6	156.9	38.8	28.5
10	96.6	111.0	33.1	31.0	3.20	3.44	104.6	122.1	30.6	28.2
11	55.2	100.0	22.0	17.0	1.21	1.70	34.9	87.2	34.8	19.5
12	44.4	61.8	17.7	13.8	0.786	0.853	34.9	52.3	22.5	16.3
13	65.9	90.4	28.1	20.6	1.85	1.86	52.3	78.5	35.4	23.7
14	68.7	94.0	39.1	24.3	2.69	2.28	52.3	78.5	51.3	29.1
15	70.2	92.4	20.4	19.2	1.43	1.77	52.3	78.5	27.4	22.6

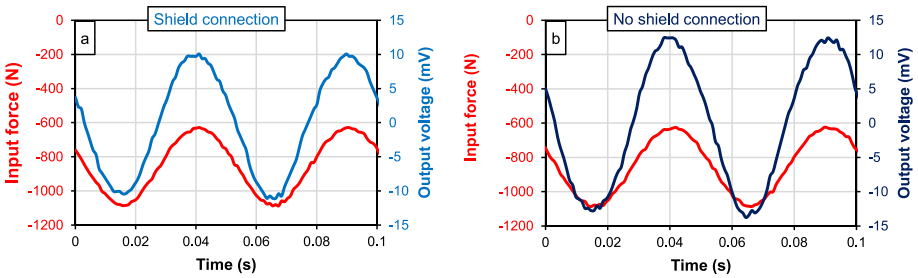

Fig. 10. Piezoelectric output vs compressive force.

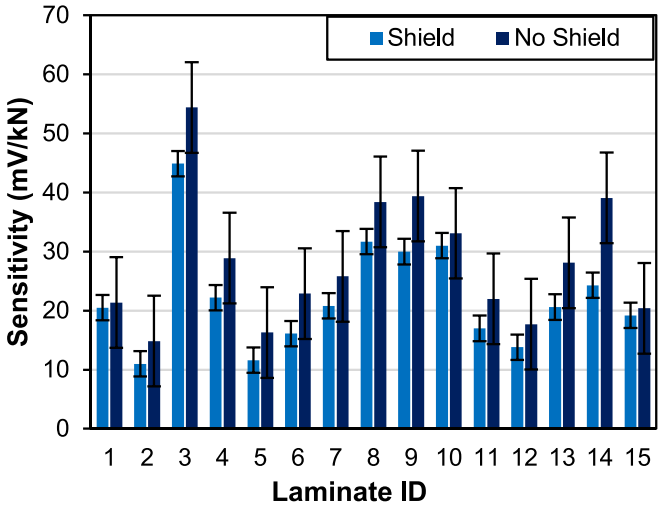

Fig. 11. Sensitivity values of the self-sensing composite laminates.

As it is well established in the piezoelectric theory [22], if the time constant of the acquisition circuit *RC* is much higher than the period of the sinusoidal compressive force, the piezoelectric strain coefficient of the composite laminates d_{33}^{c} can be obtained according to Equation (1). The d_{33}^{C} was calculated for each self-sensing laminate for both the shielded and no-shielded configurations ($d_{33_{shield}}^{C}$ and $d_{33_{no\ shield}}^{C}$), as reported in Table 4.

$$d_{33}^{C} = \frac{V(t)^{*}C}{F(t)} \tag{1}$$

As observable in Table 4, the $d_{33_{shield}}^{C}$ and $d_{33_{no\ shield}}^{C}$ are almost equal for each configuration, with an $R^2 = 98.5\%$. Indeed the composite piezoelectric constant is a specific property of the laminate composed by the piezoelectric nanofibers and GFRP plies enclosed between the signal electrodes, which is independent of the capacitance of the whole system. Therefore, here we can assume that $d_{33_{shield}}^{C} \cong d_{33_{no\ shield}}^{C} = d_{33}^{C}$.

3.2.3. Lumped electrical circuit

The behavior of the self-sensing piezoelectric composite laminates fabricated in this work can be modeled by defining an equivalent lumped electrical circuit, as shown in Fig. 12. The lumped circuit aims to model the sensitivity values of the laminates, starting from the electrical properties of the constituents between the signal electrodes (ε^{P} and ε^{G}) and the d_{33}^{c} of the laminates. The circuit was also designed to model the sensitivity of the laminates whether the shield electrodes are grounded or left floating. Since the output voltage and the compressive force of the graphs of Fig. 10 are in phase and the time constant of the *RC* circuit is much higher than the period of the sinusoidal compressive force, all the circuit impedances are represented by the capacitive contribution only. The lumped circuit can be represented and solved by using phasors.

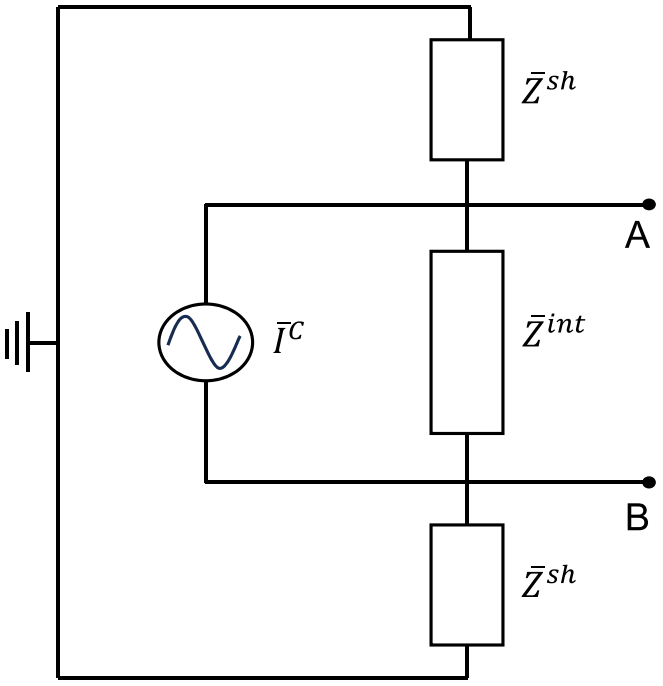

Fig. 12. Equivalent circuit of series model.

The portion of laminate between the signal electrodes can be modeled as the parallel connection between a current generator in phasor form $\bar{I}^{C} = j\omega\bar{F}_3 d_{33}^{C}$ (in time domain form $I^{C} = \frac{dF_3}{dt} d_{33}^{C}$) and the impedance $\bar{Z}^{int} = -j\frac{1}{\omega C^{int}}$, according to [22]. C^{int} is the capacitance of the portion of laminate between the signal electrodes, and it comprises both the contributions of the P(VDF-TrFE) nanofibers and the GFRP plies. Therefore, C^{int} could be modeled as the series connection of the capacitance of the GFRP layers C^{G} and the P(VDF-TrFE) one, C^{P}. From the micrograph analyses of Fig. 9, the thickness of the P(VDF-TrFE) nanofibrous membrane is negligible due to their optimal impregnation within the epoxy resin. In addition, the permittivity values of both the materials are similar (see Table 3). As consequence, it is legitimate to consider only the contribution of C^{G}, and to assume that $C^{int} \approx C^{G}$. Therefore, the capacitance C^{int} is derived from the parallel plate capacitor formula, i.e., $C^{int} = \varepsilon^{G}\frac{A}{n_{int}tk^{G}}$, where tk^{G} is the thickness of a single ply of GFRP and *A* is the area of the signal electrodes.

In addition, to model the behavior of the amount of GFRP plies between the signal electrodes and the shield electrodes, two branches with the impedances $\bar{Z}^{sh} = -j\frac{1}{\omega C^{sh}}$ were connected in series and grounded. Since in this portion of laminate there are only GFRP plies, the capacitance of the insulating layers of GFRP between the signal electrodes and the ground electrode is $C^{sh} = \varepsilon^{G}\frac{A}{0.5n_{sh}tk^{G}}$.

By applying the Kirchhoff's laws it is possible to define the sensitivity of the self-sensing composite laminates in both the shielded (S^{C*}_{shield}) and no-shielded ($S^{C*}_{no\ shield}$) configurations, as shown in Equation (2) and Equation (3), respectively and reported in Table 4.

$$S^{C*}_{shield} = \frac{d^{C}_{33}}{C^{C*}_{shield}} \tag{2}$$

$$S^{C*}_{no\ shield} = \frac{d^{C}_{33}}{C^{C*}_{no\ shield}} \tag{3}$$

where $C^{C*}_{shield} = C^{int} + C^{sh}/2$ and $C^{C*}_{no\ shield} = C^{int}$.

The apex (*) has been superimposed onto the formula to emphasize its association to the electrical circuit model and distinguish them from the experimental ones.

From Equation (2) and Equation (3) it is observable that $S^{C*}_{no\ shield}$ is higher than S^{C*}_{shield}, due to the addition of the capacitive contribution of the shielding ($C^{sh}/2$). Hence, the higher the equivalent capacitance of the laminate the lower the sensitivity. Theoretically, a large amount of GFRP plies between signal and shield electrodes (n_{sh}) leads to enhanced sensitivity value. Moreover, another possible factor which influences the capacitance is the electrodes' area. For instance, the fabrication of a large surface self-sensing laminate could lower its sensitivity, due to the increase of capacitance.

Table 4 is divided in a first experimental section and a second one which refers to the lumped electrical circuit model. Therefore, correlations between the experimental and the lumped electrical circuit model sections can be deduced. The experimental capacitances of the self-sensing composite laminates measured in the shielded configuration (C^{C}_{shield}) match the ones predicted by the lumped circuit model with a coefficient of correlation $R^2 = 93\%$. On the other hand, in the case of the no-shielded configuration, the R^2 increases up to 95.5 %.

Through the modeled capacitances and the d^{C}_{33} of the laminates it was possible to determine the sensitivity values S^{C*}_{shield} and $S^{C*}_{no\ shield}$. Those sensitivities match the experimentally measured ones (S^{C}_{shield} and $S^{C}_{no\ shield}$) with a coefficient of determination $R^2 = 96\%$ and $R^2 = 88\%$, respectively. The lower coefficient of determination in the no-shield configuration can be ascribed to the presence of triboelectric noise and electromagnetic interference in the experimental measurements, which instead are not taken into account in the designed model.

3.3. Function response surface

As mentioned in Section 2.1.4, the sensitivity was used as response of the full quadratic regression model. The mathematical polynomial function was exploited to generate a response surface which describes the behavior of the self-sensing composite laminates, as function of the variables *Gr*, n_{int} and n_{sh}. A generic form for a typical response surface function for the three input variables is in the following form:

$$y = b_0 + b_1x_1 + b_2x_2 + b_3x_3 + b_{11}x_1^2 + b_{22}x_2^2 + b_{33}x_3^2 + b_{12}x_1x_2 + b_{13}x_1x_3 + b_{23}x_2x_3 \tag{4}$$

In which y is the response variable and describes a four-dimensional surface, which depends on the independent variables x_i (also called regressors), while the b_i parameters are called coefficient regressors [44].

The results of the response surface model fitting in the form of analysis of variance (ANOVA) - calculated with the commercial software Minitab - are given in Table 5, which was made according to the guidelines of [44].

As shown in the Contribution column of the ANOVA, the whole model explains the experimental data with a coefficient of determination $R^2 = 94.05\%$, which has different contributions. In particular, the linear contribution is the most impactful one (84.83%), whereas the square and the two-way interaction ones are both around the 5 %. The importance of each coefficient of the model is described by the p-value, which is the smallest level of significance that would lead to the rejection of the significance of the parameter [44]. As usually done for the statistical tests, in this work the level of significance $\alpha = 0.05$ was adopted.[44]. Therefore, the parameters to be considered as the most important are the ones with a p-value < 0.05. For this reason, only *Gr* and n_{int} should be considered for the empirical relationship between the parameters and the sensitivity of the self-sensing composite laminates. It is clearly deductible from Table 5 that the so obtained empirical law would present a coefficient of determination equal to $R^2 = 82.92\%$. To further improve the accuracy of the model and taking into account the curvature of the response surface, the most significant parameters of the square (n^2_{int}), and the two-way interaction sections ($n_{int}Gr$) were also included in the regression model. In addition, the n_{sh} parameter was also considered to evaluate the effect of the shielding configuration, despite its p-value is higher than 0.05.

The so obtained empirical relationship between the sensitivity *S* and the variables of the model (P(VDF-TrFE) grammage *Gr*, GFRP between inner electrodes n_{int}, GFRP between signal and shielding electrodes n_{sh} expressed as coded values, as shown in Table 1) is described in Equation

Table 5
Analysis of variance, whose results are reported for each term of the mode: P(VDF-TrFE) grammage (Gr), GFRP between inner electrodes (n_{int}), GFRP between signal and shielding electrodes (n_{sh}). The columns refer to the degree of freedom (DF), the contributions to the explaining of the experimental data (Contribution), the adjusted sum of squares (Adj SS), the adjusted mean squares (Adj MS), the statistical F and P values.

Source	DF	Contribution	Adj SS	Adj MS	F-Value	P-Value
Model	**9**	**94.05 %**	**1069.37**	**118.819**	**8.78**	**0.014**
Linear	**3**	**84.83 %**	**964.52**	**321.507**	**23.75**	**0.002**
Gr	1	40.11 %	456.02	456.020	33.69	0.002
n_{int}	1	42.81 %	486.72	486.720	35.95	0.002
n_{sh}	1	1.92 %	21.78	21.780	1.61	0.260
Square	**3**	**4.10 %**	**46.64**	**15.547**	**1.15**	**0.415**
Gr^2	1	0.00 %	0.14	0.136	0.01	0.924
n^2_{int}	1	3.36 %	35.29	35.293	2.61	0.167
n^2_{sh}	1	0.74 %	8.40	8.400	0.62	0.467
2-Way Interaction	**3**	**5.12 %**	**58.21**	**19.403**	**1.43**	**0.337**
$Gr*n_{int}$	1	3.83 %	43.56	43.560	3.22	0.133
$Gr*n_{sh}$	1	0.90 %	10.24	10.240	0.76	0.424
$n_{int}*n_{sh}$	1	0.39 %	4.41	4.410	0.33	0.593
Error	**5**	**5.95 %**	**67.69**	**13.537**		
Lack-of-Fit	3	4.73 %	53.80	17.933	2.58	0.291
Pure Error	2	1.22 %	13.89	6.943		
Total	14	100.00 %				

(5) and presents a $R^2 = 92.02\%$, which is only 2 % lower than the R^2 of the full quadratic model.

$$S = 20.61 + 7.55Gr - 7.80n_{int} + 1.65n_{sh} + 3.09n_{int}^2 - 3.30n_{int}Gr \quad (5)$$

In the first instance, using the coded values for each variable, it is feasible to determine the influence of each factor simply by comparing the regressor coefficients of each term. In particular, the larger the coefficient the more incident the term.

From Equation (5), it is possible to generate a visual interpretation of the predicted model, by using the response surfaces and the contour plots.

The response surface plots are three-dimensional plots that shows the relationship between the sensitivity and the other two independent variables. Since the model of Equation (5) presents three independent variables, Fig. 13 shows three graphs, holding fixed one of the three independent variables at a time for each of them. In each graph, the hold value was set at the central point of the design space (i.e., Gr=20 g/m^2; n_{int}=4; n_{sh}=4).

The contour plots are a two-dimensional display of the surface plots, where the sensitivity values are drawn as isolines in the plane of the independent values. When the isolines of the contour plot are straight and parallel to each other, the variables of the specific contour plot do not have any interactions. On the other hand, the greater the curvature of the isolines, the greater the interactions and the high order effects between the variables. The interactions between the variables of the proposed model are then visible in the contour plots of Fig. 14.

All the contour plots of Fig. 14 have been done by spacing each sensitivity isoline with a step equal to 4 mV/kN. As observable from the Gr vs n_{int} graph, these two variables have a considerable impact on the sensitivity, as the isolines are close to each other and the sensitivity variation is remarkable even for low variation of Gr and n_{int}. For sensitivity isolines higher than 20 mV/kN, the effect of the linear terms is preponderant and the isolines are almost parallel lines. In this region, the isolines are 45°-oriented as consequence of similar absolute values of the regression coefficients of Gr and n_{int}, i.e., 7.55 and −7.80 respectively, as shown Equation (5). On the other hand, for low Gr values (i.e., 10 and 15 g/m^2), curvatures of the isolines are visible as the quadratic term of n_{int} is the most important. This behavior is clearly observable also in the surface plot with n_{sh} as hold value of Fig. 13, where the area with the grater curvature is the one with high values of n_{int} and low values of Gr. Due to the negative value of the coefficient of n_{int}, theoretically the absence of GFRP layers between the signal electrodes is desirable to achieve higher sensitivity values. In practice, in this typology of self-sensing laminate, the presence of GFRP layers is mandatory to electrically insulate the two signal electrodes.

Since in the function response of Equation (5) the interaction terms between n_{sh} and Gr and their quadratic effects have not been considered, the surface plot with n_{int} as hold value of Fig. 13 is a plane and the isolines of the Gr vs n_{sh} contour plot are parallel. In this case, the isoline almost vertically disposed as the regression coefficient of Gr is much higher than the n_{sh} one.

The low impact of n_{sh} is also visible in the n_{int} vs n_{sh} contour plot, where the isolines are almost vertically disposed for sensitivity values up

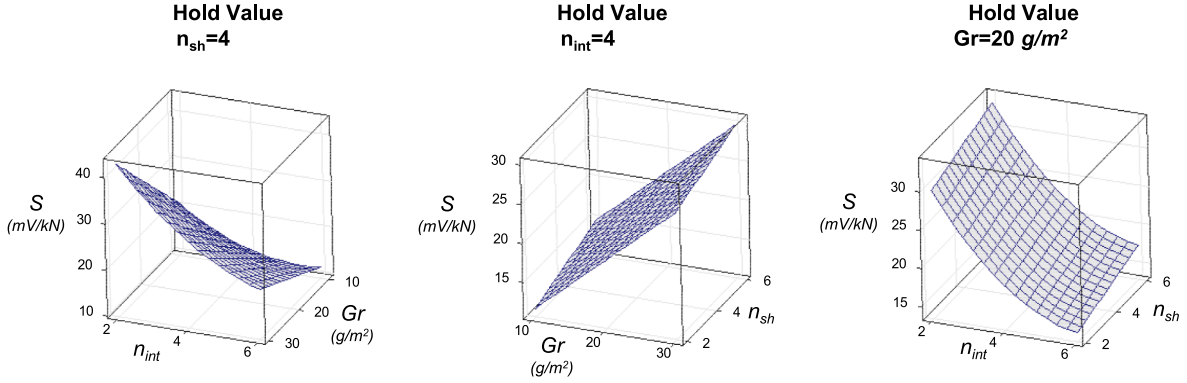

Fig. 13. Three-dimensional response surface plots, with each variable fixed at the central point of the design space.

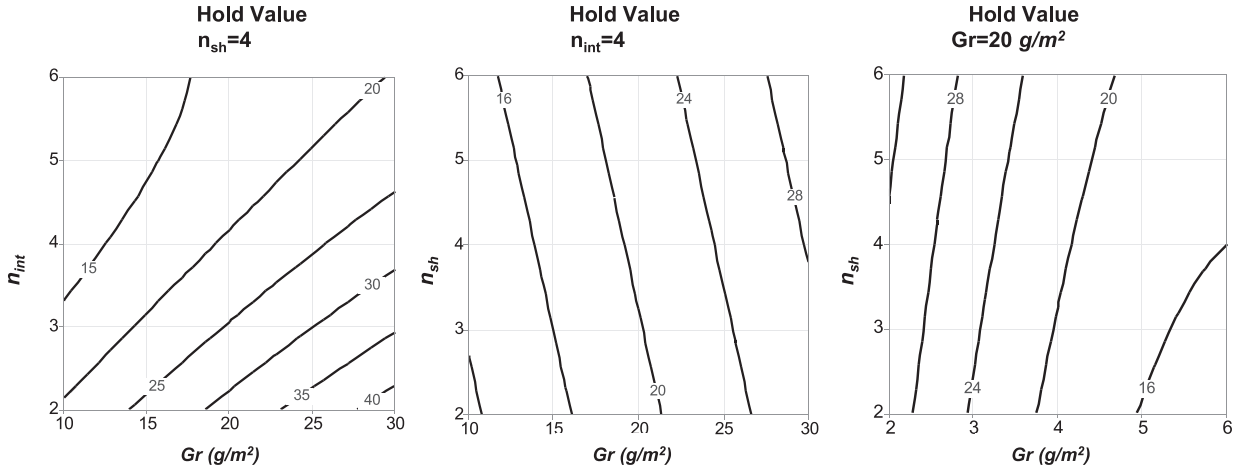

Fig. 14. Contour plots with each variable fixed at the central point of the design space.

to 20 mV/kN. By increasing n_{int}, the quadratic term n_{int}^2 is the most impactful and a curvature is observable. These considerations suggest that for low-sensible composite laminates (i.e., high amount of GFRP between the electrodes), the increasing of number of GFRP shielding plies (n_{sh}) is important to erase outer noise and increase the sensitivity.

4. Conclusions

In this study, a self-sensing composite material based on P(VDF-TrFE) nanofibers and Cu-CFRP electrodes has been successfully developed. In addition to the well-known mechanical properties, carbon fibers have been exploited as electrode to collect the piezoelectric signal generated by the nanofibers, instead of traditional metallic sheets.

Since in real applications the stacking sequence can be varied to match electrical and mechanical requirements, the experimental campaign has been conducted to study the effect of the design parameters on the piezoelectric performances of the laminates. A Box-Benken approach was adopted to optimize the experimental campaign and to define an effective regression model, which explains the effect of the parameters and their influence on the stacking sequence with a coefficient of determination of $R^2 = 92.02\,\%$. In particular, the grammage of the piezoelectric nanofibrous membrane (Gr), the amount of GFRP plies between the signal electrodes (n_{int}) and the number of GFRP plies between the signal electrodes and the shield ones (n_{sh}) have been considered as parameter of the experimental campaign. Among these, Gr and n_{int} resulted to be the most impactful on the sensitivity of the laminates, while n_{sh} presents a significant contribution only for low-sensitive laminates (i.e., sensitivity $<$ 20 mV/kN). In conclusion, to maximize the sensitivity, the Gr and n_{sh} have to be increased while n_{int} has to be decreased, as shown by the response surfaces and contour plots. The most performing laminate results to be the ID_3 with a configuration parameters of $Gr = 30g/m^2$; $n_{int} = 2$; $n_{sh} = 4$ reaching a sensitivity of 44.9 mV/kN.

Furthermore, a lumped electric circuit was designed to provide an analytical explanation of the piezoelectric behavior of the laminates. It has been demonstrated that the presence of shielding electrodes increases the capacitance of the whole self-sensing laminate and for this reason reduces the sensitivity. This paper represents a significative step towards a better understanding of the correlation between the stacking sequences and the sensing performances. This work can provide a good methodology to identify the optimal stacking sequence configuration to match the sensitivity and mechanical requirements with a reduced number of samples. Moreover, the developed self-sensing laminate can be used in SHM applications, such as impact detection or even localization via Lamb wave propagation.

CRediT authorship contribution statement

Francesco Mongioì: Writing – review & editing, Writing – original draft, Methodology, Investigation, Formal analysis, Conceptualization. **Giacomo Selleri:** Writing – review & editing, Writing – original draft, Methodology, Investigation, Formal analysis, Conceptualization. **Tommaso Maria Brugo:** Writing – review & editing, Writing – original draft, Project administration, Methodology, Investigation, Funding acquisition, Formal analysis, Conceptualization. **Emanuele Maccaferri:** Supervision, Methodology, Conceptualization. **Davide Fabiani:** Supervision, Conceptualization. **Andrea Zucchelli:** Supervision, Funding acquisition, Conceptualization.

Declaration of competing interest

The authors declare that they have no known competing financial interests or personal relationships that could have appeared to influence the work reported in this paper.

Data availability

Data will be made available on request.

Acknowledgments

This research was funded by PNR - Alma Idea 2022 (CUP J45F21002000001) and it was financed by the European Union - NextGenerationEU National Sustainable Mobility Center (CN00000023) Spoke 11 - Innovative Materials & Lightweighting.

References

[1] Abrate S. Impact Dynamics. In: Abrate S, editor. Impact Engineering of Composite Structures. Springer Vienna; 2011. p. 71–96. https://doi.org/10.1007/978-3-7091-0523-8_3.
[2] Cai J, Qiu L, Yuan S, Shi L, Liu P, Liang D. Structural Health Monitoring for Composite Materials. In: in Composites and Their Applications, no. February 2017; 2012. https://doi.org/10.5772/48215.
[3] Takeda N, Okabe Y, Kuwahara J, Kojima S, Ogisu T. Development of smart composite structures with small-diameter fiber Bragg grating sensors for damage detection: Quantitative evaluation of delamination length in CFRP laminates using Lamb wave sensing. Compos Sci Technol Dec. 2005;65(15–16):2575–87. https://doi.org/10.1016/J.COMPSCITECH.2005.07.014.
[4] Oromiehie E, Prusty BG, Compston P, Rajan G. Characterization of process-induced defects in automated fiber placement manufacturing of composites using fiber Bragg grating sensors. Struct Heal Monit 2018;17(1):108–17. https://doi.org/10.1177/1475921716685935.
[5] Oromiehie E, Prusty BG, Compston P, Rajan G. In situ process monitoring for automated fibre placement using fibre Bragg grating sensors. Struct Heal Monit 2016;15(6):706–14. https://doi.org/10.1177/1475921716658616.
[6] Masmoudi S, El Mahi A, Turki S. Use of piezoelectric as acoustic emission sensor for in situ monitoring of composite structures. Compos Part B Eng Oct. 2015;80:307–20. https://doi.org/10.1016/J.COMPOSITESB.2015.06.003.
[7] Chilles JS, Croxford A, Bond IP. The influence of tensile stress on inductively coupled piezoceramic sensors embedded in fibre-reinforced plastics. Struct Heal Monit 2021;20(5):2261–73. https://doi.org/10.1177/1475921720926166.
[8] Shivakumar K, Bhargava A. Failure Mechanics of a composite laminate embedded with a fiber optic sensor. J Compos Mater 2005;39(9):777–98. https://doi.org/10.1177/0021998305048156.
[9] Cheng J, Qian C, Zhao M, Lee R, Zhang T-Y. Effects of electric fields on the bending behavior of PZT-5H piezoelectric laminates. Smart Mater Struct 2000;9(6):824. https://doi.org/10.1088/0964-1726/9/6/312.
[10] Li HN, Li DS, Song GB. Recent applications of fiber optic sensors to health monitoring in civil engineering. Eng Struct 2004;26(11):1647–57. https://doi.org/10.1016/j.engstruct.2004.05.018.
[11] Lin B, Giurgiutiu V. Modeling and testing of PZT and PVDF piezoelectric wafer active sensors. Smart Mater Struct 2006;15(4):1085–93. https://doi.org/10.1088/0964-1726/15/4/022.
[12] Narita F, Nagaoka H, Wang Z. Fabrication and impact output voltage characteristics of carbon fiber reinforced polymer composites with lead-free piezoelectric nano-particles. Mater Lett 2019;236:487–90. https://doi.org/10.1016/j.matlet.2018.10.174.
[13] Spinelli G, Lamberti P, Tucci V, Vertuccio L, Guadagno L. Experimental and theoretical study on piezoresistive properties of a structural resin reinforced with carbon nanotubes for strain sensing and damage monitoring. Compos Part B Eng Jul. 2018;145:90–9. https://doi.org/10.1016/J.COMPOSITESB.2018.03.025.
[14] Wichmann MHG, Buschhorn ST, Gehrmann J, Schulte K. Piezoresistive response of epoxy composites with carbon nanoparticles under tensile load. Phys Rev B - Condens Matter Mater Phys 2009;80(24):1–8. https://doi.org/10.1103/PhysRevB.80.245437.
[15] Zhang Z, Wei H, Liu Y, Leng J. Self-sensing properties of smart composite based on embedded buckypaper layer. Struct Heal Monit 2015;14(2):127–36. https://doi.org/10.1177/1475921714568405.
[16] Gino E, et al. On the design of a piezoelectric self-sensing smart composite laminate. Mater Des 2022;219:110783. https://doi.org/10.1016/j.matdes.2022.110783.
[17] Mahato B, Lomov SV, Jafarypouria M, Owais M, Abaimov SG. Hierarchical toughening and self-diagnostic interleave for composite laminates manufactured from industrial carbon nanotube masterbatch. Compos Sci Technol Oct. 2023;243:110241. https://doi.org/10.1016/J.COMPSCITECH.2023.110241.
[18] Philibert M, Chen S, Wong VK, Yao K, Soutis C, Gresil M. Direct-write piezoelectric transducers on carbon-fiber-reinforced polymer structures for exciting and receiving guided ultrasonic waves. IEEE Trans Ultrason Ferroelectr Freq Control 2021;68(8):2733–40. https://doi.org/10.1109/TUFFC.2021.3073131.
[19] Philibert M, Chen S, Yao K, Soutis C, Gresil M. Direct-write piezoelectric ultrasonic transducers for impact damage detection in composite plates. 9th European Workshop on Structural Health Monitoring, EWSHM 2018. 2018. no. November.
[20] De Rosa IM, Sarasini F. Use of PVDF as acoustic emission sensor for in situ monitoring of mechanical behaviour of glass/epoxy laminates. Polym Test Sep. 2010;29(6):749–58. https://doi.org/10.1016/J.POLYMERTESTING.2010.04.006.

[21] Caneva C, De Rosa IM, Sarasini F. Monitoring of impacted aramid-reinforced composites by embedded PVDF acoustic emission sensors. Strain 2008;44:308–16. https://doi.org/10.1111/j.1475-1305.2007.00374.
[22] Brugo TM, et al. Self-sensing hybrid composite laminate by piezoelectric nanofibers interleaving. Compos Part B Eng 2021;212(February):108673. https://doi.org/10.1016/j.compositesb.2021.108673.
[23] Saghafi H, Brugo T, Minak G, Zucchelli A. The effect of PVDF nanofibers on mode-I fracture toughness of composite materials. Compos Part B Eng 2015;72:213–6. https://doi.org/10.1016/j.compositesb.2014.12.015.
[24] Ramakrishna S, Fujihara K, Teo WE, Lim TC, Ma Z. An introduction to electrospinning and nanofibers. World Scientific Publishing Co 2005. https://doi.org/10.1142/5894.
[25] Park JS. Electrospinning and its applications. Adv Nat Sci Nanosci Nanotechnol 2010;1(4):pp. https://doi.org/10.1088/2043-6262/1/4/043002.
[26] Calavalle F, Zaccaria M, Selleri G, Cramer T, Fabiani D, Fraboni B. Piezoelectric and electrostatic properties of electrospun PVDF-TrFE nanofibers and their role in electromechanical transduction in nanogenerators and strain sensors. Macromol Mater Eng 2020;305(7):1–8. https://doi.org/10.1002/mame.202000162.
[27] Mandal D, Yoon S, Kim KJ. Origin of piezoelectricity in an electrospun poly (vinylidene fluoride-trifluoroethylene) nanofiber web-based nanogenerator and nano-pressure sensor. Macromol Rapid Commun 2011;32(11):831–7. https://doi.org/10.1002/marc.201100040.
[28] Palazzetti R, Zucchelli A. Electrospun nanofibers as reinforcement for composite laminates materials – a review. Compos Struct Dec. 2017;182:711–27. https://doi.org/10.1016/J.COMPSTRUCT.2017.09.021.
[29] Mahato B, Lomov SV, Shiverskii A, Owais M, Abaimov SG. A review of electrospun nanofiber interleaves for interlaminar toughening of composite laminates. Polymers (Basel) Mar. 2023;15(6):1380. https://doi.org/10.3390/polym15061380.
[30] Brugo T, Palazzetti R. The effect of thickness of Nylon 6,6 nanofibrous mat on Modes I-II fracture mechanics of UD and woven composite laminates. Compos Struct Oct. 2016;154:172–8. https://doi.org/10.1016/J.COMPSTRUCT.2016.07.034.
[31] Zarei H, Brugo T, Belcari J, Bisadi H, Minak G, Zucchelli A. Low velocity impact damage assessment of GLARE fiber-metal laminates interleaved by Nylon 6,6 nanofiber mats. Compos Struct May 2017;167:123–31. https://doi.org/10.1016/J.COMPSTRUCT.2017.01.079.
[32] Selleri G, et al. Self-sensing composite material based on piezoelectric nanofibers. Mater Des Jul. 2022;219:110787. https://doi.org/10.1016/J.MATDES.2022.110787.
[33] Naderiallaf H, Seri P, Montanari GC. Designing a HVDC insulation system to endure electrical and thermal stresses under operation. Part I: partial discharge magnitude and repetition rate during transients and in DC steady state. IEEE Access 2021;9:35730–9. https://doi.org/10.1109/ACCESS.2021.3062440.
[34] Selleri G, et al. Study on the polarization process for piezoelectric nanofibrous layers. Annu Rep - Conf Electr Insul Dielectr Phenomena, CEIDP 2021;vol. 2021-Decem:61–4. https://doi.org/10.1109/CEIDP50766.2021.9705470.
[35] Waller D, Safari A. Corona poling of pzt ceramics and flexible piezoelectric composites. Ferroelectrics 1988;87(1):189–95. https://doi.org/10.1080/00150198808201381.
[36] Waller D, Iqbal T, Safari A. Poling of lead zirconate titanate ceramics and flexible piezoelectric composites by the corona discharge technique. J Am Ceram Soc 1989;72(2):322–4. https://doi.org/10.1111/j.1151-2916.1989.tb06125.x.
[37] Gasperini L, Selleri G, Pegoraro D, Fabiani D. Corona poling for polarization of nanofibrous mats advantages and open issues. In: 2022 IEEE Conf. Electr. Insul. Dielectr. Phenom.; 2022. p. 31–4. https://doi.org/10.1109/CEIDP55452.2022.9985267.
[38] Giacometti JA, Oliveira ON. Corona charging of polymers. IEEE Trans Electr Insul 1992;27(5):924–43. https://doi.org/10.1109/14.256470.
[39] Safarova V, Gregr J. Electrical conductivity measurement of fibers and yarns. In: 7th Int Conf; 2010. p. 2–9.
[40] Wang Z, Kurita H, Nagaoka H, Narita F. Potassium sodium niobate lead-free piezoelectric nanocomposite generators based on carbon-fiber-reinforced polymer electrodes for energy-harvesting structures. Compos Sci Technol 2020;199(July):108331. https://doi.org/10.1016/j.compscitech.2020.108331.
[41] Qiu L, Yuan S, Shi X, Huang T. Design of piezoelectric transducer layer with electromagnetic shielding and high connection reliability. Smart Mater Struct 2012;21(7):pp. https://doi.org/10.1088/0964-1726/21/7/075032.
[42] Wang G, et al. Damage detection for structural health monitoring using ultra-sensitive flexible piezoelectret sensors. Struct Heal Monit 2023;22(4):pp. https://doi.org/10.1177/14759217221137807.
[43] Ferreira SLC, et al. Box-Behnken design : an alternative for the optimization of analytical methods. Anal Chim Acta 2007;597(2):179–86. https://doi.org/10.1016/j.aca.2007.07.011.
[44] Montgomery DC. Design and analysis of experiments. 9 Edition. Wiley; 2017.